Phys Chem Minerals (2004) 31: 633–642
DOI 10.1007/s00269-004-0420-0

ORIGINAL PAPER

D. Lenaz · H. Skogby · F. Princivalle · U. Hålenius

Structural changes and valence states in the $MgCr_2O_4$–$FeCr_2O_4$ solid solution series

Received: 10 May 2004 / Accepted: 1 August 2004

Abstract The influence on the structure of $Fe^{2+} \rightarrow Mg$ substitution was studied in synthetic single crystals belonging to the $MgCr_2O_4$–$FeCr_2O_4$ series produced by flux growth at 900–1200 °C in controlled atmosphere. Samples were analyzed by single-crystal X-ray diffraction, electron microprobe analyses, optical absorption-, infrared- and Mössbauer spectroscopy. The Mössbauer data show that iron occurs almost exclusively as $^{IV}Fe^{2+}$. Only minor Fe^{3+} (<0.005 apfu) was observed in samples with very low total Fe. Optical absorption spectra show that chromium with few exceptions is present as a trivalent cation at the octahedral site. Additional absorption bands attributable to Cr^{2+} and Cr^{3+} at the tetrahedral site are evident in spectra of end-member magnesiochromite and solid-solution crystals with low ferrous contents. Structural parameters a_0, u and T–O increase with chromite content, while the M–O bond distance remains nearly constant, with an average value equal to 1.995(1) Å corresponding to the Cr^{3+} octahedral bond distance. The ideal trend between cell parameter, T–O bond length and Fe^{2+} content (apfu) is described by the following linear relations: $a_0 = 8.3325(5) + 0.0443(8)Fe^{2+}$ (Å) and T–O $= 1.9645(6) + 0.033(1)Fe^{2+}$ (Å) Consequently, Fe^{2+} and Mg tetrahedral bond lengths are equal to 1.998(1) Å and 1.965(1) Å, respectively.

Keywords $MgCr_2O_4$ · $FeCr_2O_4$ spinels · Single-crystal XRD · EPMA · OAS · Mössbauer

D. Lenaz (✉) · F. Princivalle
Dipartimento di Scienze della Terra, via Weiss 8,
34127 Trieste, Italy
Tel: +390405582218
Fax: +390405582213
e-mail: lenaz@univ.trieste.it

H. Skogby · U. Hålenius
Department of Mineralogy, Swedish Museum of Natural History,
SE-10405 Stockholm, Sweden

Introduction

The spinel structure is based on a nearly ideal cubic close-packed array of oxygen atoms with tetrahedral (T) and octahedral (M) cavities. In common 2-3 spinels, one eighth of the T sites and one half of the M sites are occupied by heterovalent cations A and B in the ratio AB_2O_4, where A = (Mg, Fe^{2+}, Zn, Mn^{2+}) and B = (Al, Fe^{3+}, Cr^{3+}). In general, spinels do not show the idealized configuration, with A cations in T sites and B cations in M sites. Commonly there exists octahedral–tetrahedral disorder of A and B cations depending on thermal history. Consequently, the crystal chemistry of spinels is described by the general formula $^{IV}(A_{1-i}B_i)^{VI}(A_iB_{2-i})O_4$, where '$i$' refers to the inversion parameter. There are two ordered configurations stable at low temperature, one with $i = 0$ (normal spinel; e.g. $MgAl_2O_4$, $FeAl_2O_4$, $MgCr_2O_4$, $FeCr_2O_4$) and one with $i = 1$ (inverse spinel; e.g. $MgFe_2O_4$, $FeFe_2O_4$). With increasing temperature, disorder takes place, i.e. A and B cations undergo increasing intersite exchange over the three cation sites per formula unit. Modifications of T–O and M–O bond distances to accommodate various chemical compositions and/or cation distribution determine variations in the oxygen positional parameter u and the cell edge a_0 (Lavina et al. 2002).

In geological environments $MgCr_2O_4$–$FeCr_2O_4$ end members are very common components of spinel solid solutions. In particular, Cr is an essential constituent of many spinels in mafic and ultramafic igneous and metamorphic rocks of the crust and the upper mantle. Even if Cr-bearing spinels typically occur as accessory phases, they are widely considered as petrogenetic indicators (Irvine 1965, 1967; Evans and Frost 1975; Dick and Bullen 1984; Sack and Ghiorso 1991; Barnes and Roeder 2001), given the general relationships between spinel chemistry, rock type and petrological processes. New knowledge has been achieved through Fe–Mg exchange reactions involving Cr-spinels, olivine and orthopyroxene geothermometry (Fujii 1977; Fabries 1979),

geobarometry of upper mantle/lower crustal phase transition (O'Neill 1981; 'Neill and Wall 1987), compositional zoning as indicator of magmatic processes (Scowen et al. 1991; Peltonen 1995) or reaction progress and fluid evolution in the metamorphic system (Evans and Frost 1975; Barnes 2000) and silicate inclusion compositions and their relationships with the genetic environment (Kamenetsky 1996; Kamenetsky et al. 2001).

Due to the chemical complexity frequently observed in natural spinels and the difficulties in precise site assignment of the major cations, synthetic analogues of well-defined compositions are often studied.

In the present case, a flux-growth method was used to obtain high- quality spinel crystals with compositions corresponding to magnesiochromite $MgCr_2O_4$ and chromite $FeCr_2O_4$ end members and their solid solutions. To our knowledge, few structural studies have been performed on the end members as powders and none on single crystals. The complete series has never been studied in spite of the possibility of obtaining information on ionic radii of Mg and Fe^{2+} at the T site under conditions of complete Cr^{3+} occupancy of the M site. In fact, the large excess octahedral crystal field stabilization energy of Cr^{3+} [Δ $CFSE_{(oct\text{-}tet)}$ is about 160 kJ mol^{-1}; O'Neill and Navrotsky 1984] should ensure that Cr-bearing spinels have an almost completely normal cation distribution (Urusov 1983). Consequently, all the differences in a_0 and T–O values for the spinels are caused by Mg replacement by Fe^{2+}.

Single-crystal X-ray diffraction and electron microprobe analyses were used in this study for crystal-chemical characterization of the $MgCr_2O_4$–$FeCr_2O_4$ series. Spectroscopic methods (optical absorption-, FTIR- and Mössbauer spectroscopy) were also utilized to constrain cation valency and distribution in the studied samples.

Experimental

Crystal growth

Single crystals along the magnesiochromite-chromite join were synthesized using a flux-growth method. Analytical grade MgO, Cr_2O_3, Fe_2O_3 powders were dehydrated and dried at 900 °C for 12 h before mixing with $Na_2B_4O_7$, used as flux compound. Two samples of the $MgCr_2O_4$ end member were synthesized, one with a stoichiometric starting composition (MgCr5) and another with the double amount of the MgO component (MgCr9). About 6 g of starting material was ground under acetone in an agate mortar and mixed with a flux/nutrient ratio ranging from 2.2 to 3.2 depending on Cr and Fe^{2+} contents. The mixture was loaded in a 10-cc Pt/Au (5%) crucible which was covered by Pt foil. For Fe-containing samples, thermal runs were conducted under controlled atmosphere in an ENTECH vertical tube furnace with programmable temperature controller, whereas a standard muffle furnace was used for Fe-free samples. In order to obtain a homogeneous melt, the load was heated at 1200 °C for 24 h. Subsequently, the temperature was linearly decreased to 900 °C with 4 °C h^{-1} cooling rates. The reducing atmosphere was created by a continuous flow of high-purity CO_2 and H_2 gases into the furnace. The CO_2:H_2 ratio was maintained by TYLAN flow controllers and was kept constant at 1:2. Oxygen fugacity ranged from 10^{-11} to 10^{-17} bars at 1200 and 900 °C, respectively. The thermal runs were ended by turning off the furnace and the product was allowed to cool rapidly to room temperature. Products consisted of spinel, borate and eskolaite crystals dispersed in a boron-rich glass. By dissolving the glass in warm and dilute HCl (10%) solution, the products were reduced to eskolaite and euhedral to subhedral octahedra of dark spinels. Further details can be found in Lenaz and Skogby (2003).

X-ray single-crystal diffraction and microprobe analyses

X-ray diffraction data of the euhedral synthetic spinels were recorded on an automated KUMA-KM4 (κ-geometry) diffractometer, using MoKα radiation, monochromatized by a flat graphite crystal.

Data collection was made, according to Della Giusta et al. (1996), up to 110°of 2θ in the ω - 2θ scan mode, scan width 1.8° 2θ, counting time from 20 to 50 s, depending on peak standard deviation. Twenty four equivalent reflections of (12 8 4) (about 80° of 2θ) were accurately centred at both sides of 2θ, and the α_1 peak barycentre was used for cell-parameter determination. Diffraction intensities were corrected for Lorentz, polarization and absorption factor and then merged to obtain a set of independent reflections.

Structural refinement using the SHELX-93 program (Sheldrick 1993) was carried out against Fo^2_{hkl} in the $FD\bar{3}m$ space group (with origin at −3 m), since no evidence of different symmetry appeared. During structural refinement, variable parameters were: scale factor, oxygen positional parameter, tetrahedral and octahedral site occupancies, anisotropic thermal displacement parameter (U) and secondary extinction coefficient (Table 1). Only the isotropic U factors values are reported, as the off-diagonal terms are very small and close to their standard deviation, which is usual for the spinel structure. Off-diagonal terms are twice the standard deviation only in some refinements (Fe2-50 = −67(24) $Å^2 10^{-4}$; Fe2-60 = −50(14) $Å^2 10^{-4}$; Fe2-70 = −44(21) $Å^2 10^{-4}$).

Scattering factors were taken from the International Tables for Crystallography (1974) and Tokonami (1965). Best results were obtained using neutral scattering curves for Cr in the M site and Mg vs. Fe^{2+} in the T site, with the constraints of full site occupancy, whereas oxygen was considered to be partly ionized.

After X-ray data collection, the same crystals used for X-ray data collection were mounted on glass slides, polished and carbon-coated for electron microprobe analyses on a CAMECA-CAMEBAX microprobe operating at 15 kV and 15 nA. A 20-s counting time was used for both peak and total background. Synthetic oxide standards (MgO, FeO, Cr_2O_3) were used. Raw data were reduced by PAP-type correction software provided by CAMECA (Table 2). As structural parameters of MgCr9 (magnesiochromite end member) are very close to those of MgCr5 (magnesiochromite end member) and it is iron-free, no chemical analyses were performed on it.

Additional EMP analyses were obtained on a few samples studied by spectroscopic methods only. These analyses were performed on a Cameca SX50 instrument (Uppsala University) following procedures described in Hålenius et al. (2002).

Optical absorption spectroscopy

Optical absorption spectra in the UV/VIS range (400–2200 nm) of the samples with Fe contents in the range 0.00–0.38 atoms per formula units (apfu) were obtained at room temperature from double-sided polished single crystals mounted on glass slides. The absorber thickness was in the range 13–95 μm as determined by means of a digital micrometer. The spectra were recorded with a Zeiss MPM800 single - beam microscope-spectrometer using Zeiss Ultrafluar 10x and 32x lenses as condenser and objective, respectively. In the UV/VIS spectral range, a 75-W Xenon arc lamp served as a light source and a photomultiplier as detector. In the

Table 1 Results of structure refinement of synthetic spinels in the $MgCr_2O_4$– $FeCr_2O_4$ series. R_{int} disagreement factor between equivalent reflections (%); Ueq_O, Ueq_M, Ueq_T equivalent thermal factors for O, M site and T site ($Å^2 10^{-4}$); *Ext* isotropic secondary extinction coefficient; R1, wR2, GooF as defined in Sheldrick (1993); *N. refl.* unique reflections from set of observed ones [$I > 3\sigma(I)$]. Estimated standard deviations *in brackets*

	MgCr5	MgCr9A	Fe2-10	Fe2-10B	Fe2-20	Fe2-20B	Fe2-30	Fe2-40
a_0 (Å)	8.3329 (1)	8.3328(5)	8.3352 (1)	8.3379(3)	8.3340(1)	8.3465 (1)	8.3415 (2)	8.3490 (1)
u	0.26116 (11)	0.26121(10)	0.26119 (7)	0.26142(7)	0.26119(9)	0.26164 (9)	0.26150 (7)	0.26157 (9)
T–O (Å)	1.965 (1)	1.966(1)	1.966 (1)	1.970(1)	1.966(1)	1.975 (1)	1.972 (1)	1.975 (1)
M–O (Å)	1.995 (1)	1.994(1)	1.995 (1)	1.994(1)	1.995(1)	1.994 (1)	1.994 (1)	1.995 (1)
Ueq_O ($Å^2 10^{-4}$)	40(2)	34(2)	39(1)	43(1)	50(3)	36(2)	42(1)	47(2)
Ueq_M ($Å^2 10^{-4}$)	28(1)	22(1)	28(1)	30(1)	36(1)	23(1)	31(1)	36(1)
Ueq_T ($Å^2 10^{-4}$)	39(2)	34(2)	44(3)	49(2)	49(3)	41(2)	50(2)	56(2)
Ext	0.033(3)	0.052(4)	0.027(1)	0.033(2)	0.032(2)	0.035(3)	0.013(1)	0.018(1)
R_{int}	3.51	5.63	3.67	3.78	3.97	4.01	3.45	4.78
N. refl	163	197	176	189	155	197	182	160
R1	2.60	2.85	2.19	2.10	1.91	2.74	2.17	2.08
*w*R2	5.94	6.05	3.93	4.53	4.12	5.89	4.09	3.99
GooF	1.279	1.297	1.329	1.334	1.113	1.365	1.345	1.183

	Fe2-45	Fe2-50	Fe2-55	Fe2-60	Fe2-70	Fe2-80	Fe2-90	Fe2-100
a_0 (Å)	8.3577 (2)	8.3462 (1)	8.3613 (2)	8.3620 (1)	8.3672 (2)	8.3710 (1)	8.3739 (2)	8.3765 (2)
u	0.26192 (7)	0.26159 (12)	0.26219 (8)	0.26207 (9)	0.26224 (12)	0.26256 (12)	0.26271 (9)	0.26265 (11)
T–O (Å)	1.982 (1)	1.975 (1)	1.987 (1)	1.985 (1)	1.989 (1)	1.994 (1)	1.997 (1)	1.997 (1)
M–O (Å)	1.995 (1)	1.995 (1)	1.994 (1)	1.995 (1)	1.995 (1)	1.993 (1)	1.993 (1)	1.994 (1)
Ueq_O ($Å^2 10^{-4}$)	43(1)	45(2)	46(2)	43(2)	47(2)	47(3)	40(2)	43(2)
Ueq_M ($Å^2 10^{-4}$)	32(1)	37(1)	36(1)	32(1)	36(1)	38(1)	29(1)	34(1)
Ueq_T ($Å^2 10^{-4}$)	56(1)	57(3)	60(2)	56(2)	66(2)	69(2)	55(2)	61(1)
Ext	0.0173(8)	0.0115(7)	0.0100(7)	0.030(2)	0.0120(9)	0.014(1)	0.030(3)	0.058(4)
R_{int}	5.06	3.64	3.91	5.32	4.45	5.91	10.17	6.72
N. refl	169	114	165	163	154	143	162	164
R1	1.87	1.93	1.81	2.19	2.42	2.68	2.80	2.58
*w*R2	3.27	3.67	3.54	3.94	4.50	4.35	4.03	5.32
GooF	1.286	1.180	1.262	1.278	1.321	1.332	1.216	1.277

Table 2 Chemical compositions of synthetic spinels in the $MgCr_2O_4$–$FeCr_2O_4$ series. Up to 15 spot analyses were performed on each crystal. Estimated standard deviations *in brackets*

	MgCr5	Fe2-10	Fe2-10B[a]	Fe2-20[a]	Fe2-20B	Fe2-30	Fe2-40	Fe2-45
MgO	20.7(3)	19.2(4)	17.7(3)	19.5(3)	11.9(3)	15.8(5)	13.3(2)	7.5(1)
FeO	–	2.5(2)	4.6(4)	0.8(3)	13.1(5)	7.4(7)	11.5(2)	20.0(4)
Cr_2O_3	78.8(9)	78.2(7)	77.3(6)	78.4(2)	74.6(6)	76.9(6)	74.5(9)	71.2(7)
Total	99.5	99.9	99.6	98.7	99.6	100.1	99.3	98.7
Mg	0.991(12)	0.927(14)	0.864(12)	0.949(13)	0.604(12)	0.779(18)	0.673(10)	0.399(5)
Fe^{2+}	–	0.067(6)	0.127(12)	0.022(7)	0.374(13)	0.204(17)	0.326(6)	0.596(9)
Cr	2.006(12)	2.004(14)	2.006(7)	2.019(8)	2.014(14)	2.012(17)	2.001(11)	2.003(10)
Total	2.997	2.998	2.997	2.990	2.992	2.995	3.000	2.998

	Fe2-50	Fe2-55	Fe2-60	Fe2-70	Fe2-80	Fe2-90	Fe2-100
MgO	13.5(2)	6.0(3)	6.6(1)	3.9(1)	2.36(9)	1.07(5)	–
FeO	11.5(6)	22.5(5)	21.8(3)	25.2(3)	28.0(4)	29.5(4)	31.6(3)
Cr_2O_3	74.7(9)	70.8(9)	71.6(9)	70.2(7)	67.9(9)	69.4(7)	66.8(6)
Total	99.7	99.3	100.0	99.3	98.26	99.97	98.4
Mg	0.679(11)	0.321(16)	0.346(7)	0.212(6)	0.131(5)	0.059(3)	–
Fe^{2+}	0.324(15)	0.674(13)	0.645(9)	0.764(10)	0.871(12)	0.909(10)	1.000(9)
Cr	1.998(16)	2.003(17)	2.006(10)	2.016(11)	1.998(13)	2.022(11)	2.000(9)
Total	3.001	2.998	2.997	2.992	3.000	2.990	3.000

[a]Analyses performed in Uppsala

NIR spectral region, 800–2200 nm (12 500–4500 cm^{-1}), a 100-W halogen lamp was used as a light source and light detection was achieved by means of a photoconductive PbS cell. Spectra were recorded at a spectral resolution of 2 nm in the UV/VIS range and 10 nm in the NIR region and the measurement spot was 30 μm. Spectroscopic data were also obtained for the MIR range (5000–2000 cm^{-1}) by means of an FTIR spectrometer (Bruker Equinox 55S) equipped with an IR microscope. These spectra were recorded

at a resolution of 8 cm^{-1} with measuring areas around 75 × 75 μm using a glowbar source, KBr beamsplitter and an MCT detector.

^{57}Fe Mössbauer spectroscopy

^{57}Fe Mössbauer spectra were obtained using a conventional spectrometer system operated in constant acceleration mode using a 50-m Ci ^{57}Co source in Rh matrix. Absorbers were prepared by grinding 6–50- mg sample material which was mixed with thermoplastic resin (transoptic powder) and pressed to discs under moderate heating. Data over the velocity range −4.5 to + 4.5 mm s^{-1} were recorded at room temperature in a multichannel analyzer using 1024 channels. The mirror-symmetric spectra were folded, velocity-calibrated against α-iron spectra, and further reduced to 256 channels before fitting using a least-squares program (Jernberg and Sundqvist 1983). Lorentzian lines, equal recoil-free fractions and equal intensity of the quadrupole components were assumed in the fitting procedure.

Results

EMP analyses frequently show spinel compositions that deviate from oxide mixture composition. This is probably caused by a combination of uptake (and release) of iron in the crucible material, and distribution of Fe and

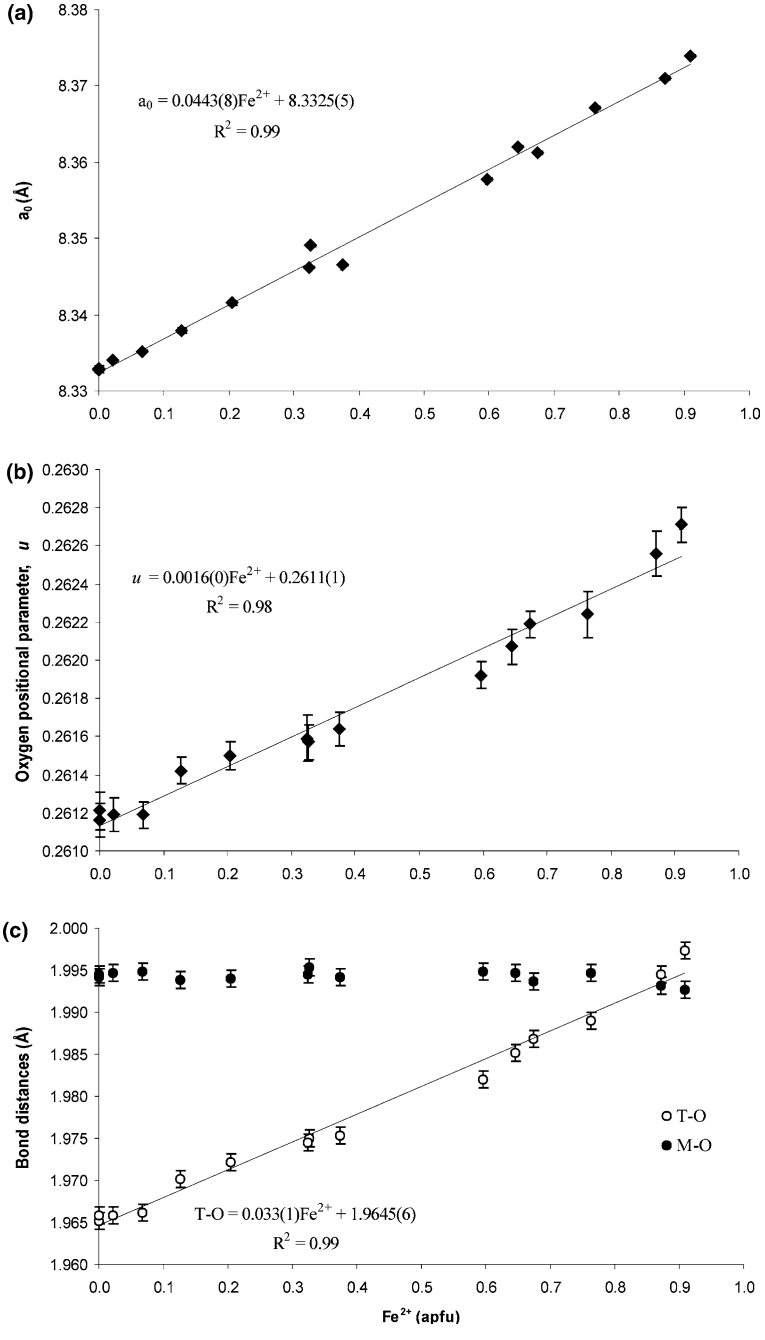

Fig. 1a–c Variations in structural parameters as a function of chromite end-member content in $MgCr_2O_4$–$FeCr_2O_4$ crystals. **a** Unit cell parameter a_0 vs. Fe^{2+} content (apfu), standard deviations are *within the symbols*. **b** Oxygen positional parameter u vs. Fe^{2+} content (apfu). **c** T–O and M–O bond distances vs. Fe^{2+} content (apfu), standard deviations equal to 2σ

Mg between the spinel and borate phases. Minor eskolaite (Cr_2O_3) inclusions were found in some samples, and intermediate samples sometimes reveal weak core to rim zonations. However, since chemical analyses were obtained from the same crystals as used for XRD data collection, the effect of these weak zonations is deemed insignificant.

Our spinel crystals are representative of the whole magnesiochromite-chromite series. On the basis of very strong Cr^{3+} site-preference energies, the M site is fully

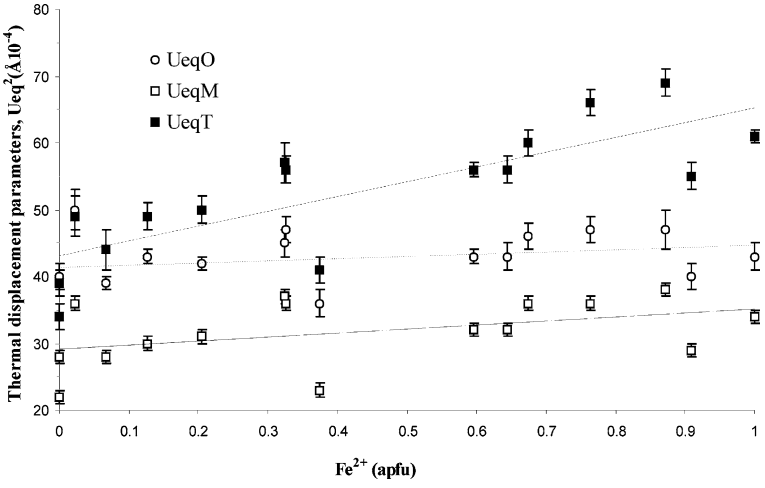

Fig. 2 Variations in thermal displacement factors *Ueq* (*O*), (*M*), (*T*) as a function of chromite end-member content in $MgCr_2O_4$–$FeCr_2O_4$ crystals. *Lines* are guides for the eye to give a qualitative impressions of overall behaviour of the *Ueq* variations

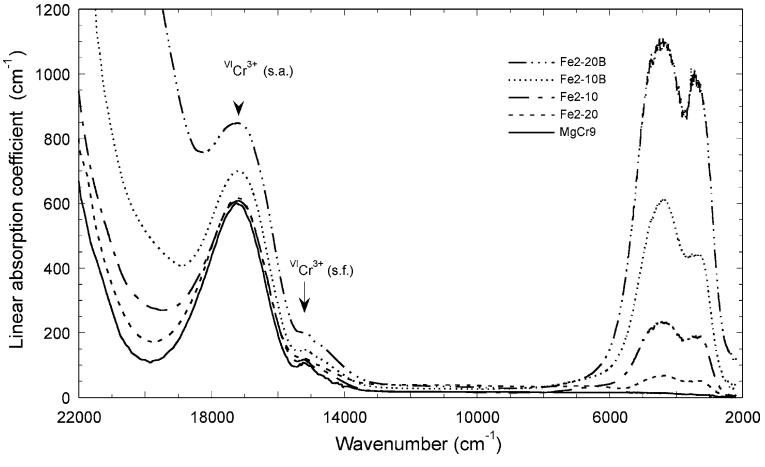

Fig. 3 Absorption spectra in the UV/VIS/IR range for $Fe_xMg_{1-x}Cr_2O_4$ ($0.00 < x < 0.37$) spinels. Bands between 2000 and 6000 cm^{-1} are caused by spin-allowed $^{IV}Fe^{2+}$ *d–d* electronic transitions. *s.a.* spin-allowed; *s.f.* spin-forbidden

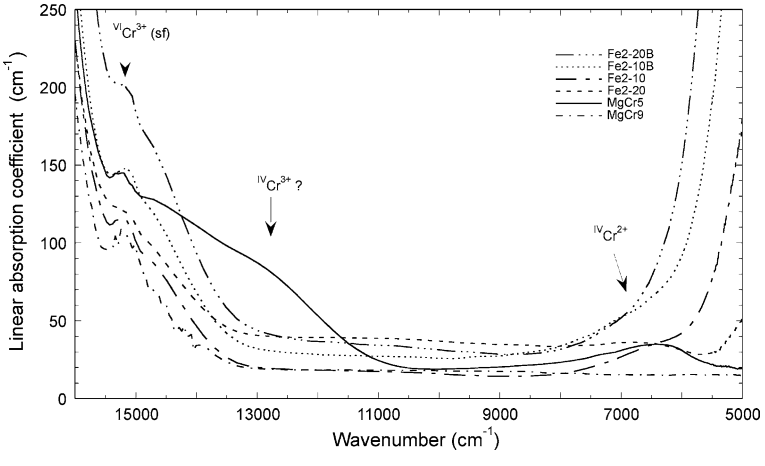

Fig. 4 Expanded part of Fig. 2 including MgCr5 sample. Additional bands assigned to $^{IV}Cr^{2+}$ and tentatively $^{IV}Cr^{3+}$ are indicated

occupied by Cr^{3+} (O'Neill and Navrotsky 1983; Urusov 1983). Consequently, crystal chemistry is defined by $Fe^{2+} \rightarrow Mg$ substitution.

Structural parameters a_0, u and T–O distance increase with chromite content (Fig. 1), while the M–O distance remains rather constant at 1.995(1) Å (Table 1), which is in good agreement with previously reported octahedral Cr^{3+}–O bond distances (Shannon 1976; O'Neill and Navrotsky 1983; Lavina et al. 2002). As a consequence, the variations of a_0 (from 8.3329(1) to 8.3765(2) Å) are essentially due to the T–O increase (from 1.965 to 1.997 Å).

The comparison of present data is possible only with those by O'Neill and Dollase (1994), who studied the crystal structures and cation distribution of $MgCr_2O_4$ from powder XRD structural refinements. Three samples of $MgCr_2O_4$ annealed at 900, 1100 and 1300 °C were all found to have $i = 0$ within two estimated standard deviations, confirming the M site preference of Cr. In addition, the lattice parameters and oxygen positional parameters were found to be between 8.3339(1) and 8.3341(1) and between 0.2612(2) and 0.2607(4), respectively. Moreover, the neutron diffraction study of $MgCr_2O_4$ carried out by Infante and Fender (1973) gave u equal to 0.2612(1). All these values are very close or equal to the parameters of the $MgCr_2O_4$ end member studied.

Equivalent thermal factors for O and M site are more or less constant (Table 1) while there is an increase of Ueq_T that seems to be related with Fe^{2+} increase (Fig. 2).

The recorded optical absorption spectra show intense and relatively broad absorption bands at ~17 200 cm^{-1} as well as in the region 5000–3000 cm^{-1} and a set of weak and narrow bands between ~14 500 and ~15 500 cm^{-1} (Fig. 3). In accordance with previous studies on Cr^{3+}-bearing spinels, the strong band at ~17 200 cm^{-1} and the weak and narrow bands at higher wavenumbers are supposed to be caused by a spin-allowed $[^4A_{2g}(F)–^4T_{2g}(F)]$ and spin-forbidden electronic *d–d* transitions in Cr^{3+} at the octahedral site, respectively (e.g. Poole 1964; Taran et al. 1994). Due to high Cr^{3+} concentrations and difficulties to prepare thin absorbers (< 10 μm), it was not possible to record the very intense high energy band at ~25 000 cm^{-1}, which is caused by a spin-allowed *d–d* transition $[^4A_{2g}(F)–^4T_{1g}(F)]$ in $^{VI}Cr^{3+}$. Only the low-energy wing of this band is observed in the present spectra. This low-energy wing is apparently intensified by a superimposed intense low-energy wing of aO–Fe^{2+} intervalence charge transfer band in spectra of $^{IV}Fe^{2+}$-rich samples. The strong and split spin-allowed IR band peaking at ~4700 cm^{-1}, which increases in intensity with increasing ferrous content, is due to spin-allowed *d–d* transitions in Fe^{2+} at the tetrahedral site (e.g. Slack et al. 1966; Gaffney 1973). In addition, a relatively broad and weak band at ~6500 cm^{-1} is observed in spectra of one of the end-member magnesiochromite samples (MgCr5) and in the samples with the lowest contents of ferrous iron (Fig. 3). This feature has been previously recorded in synthetic Mg–Cr spinels and assigned to a spin-allowed *d–d* transition $[^5T_{2g}(D)–^5E_g(D)]$ in Cr^{2+} at tetrahedral sites (e.g. Greskovich and Stubican 1966). The spectra of this $MgCr_2O_4$ end-member sample MgCr5 also reveals a weak and broad absorption band at ~13 000 cm^{-1}

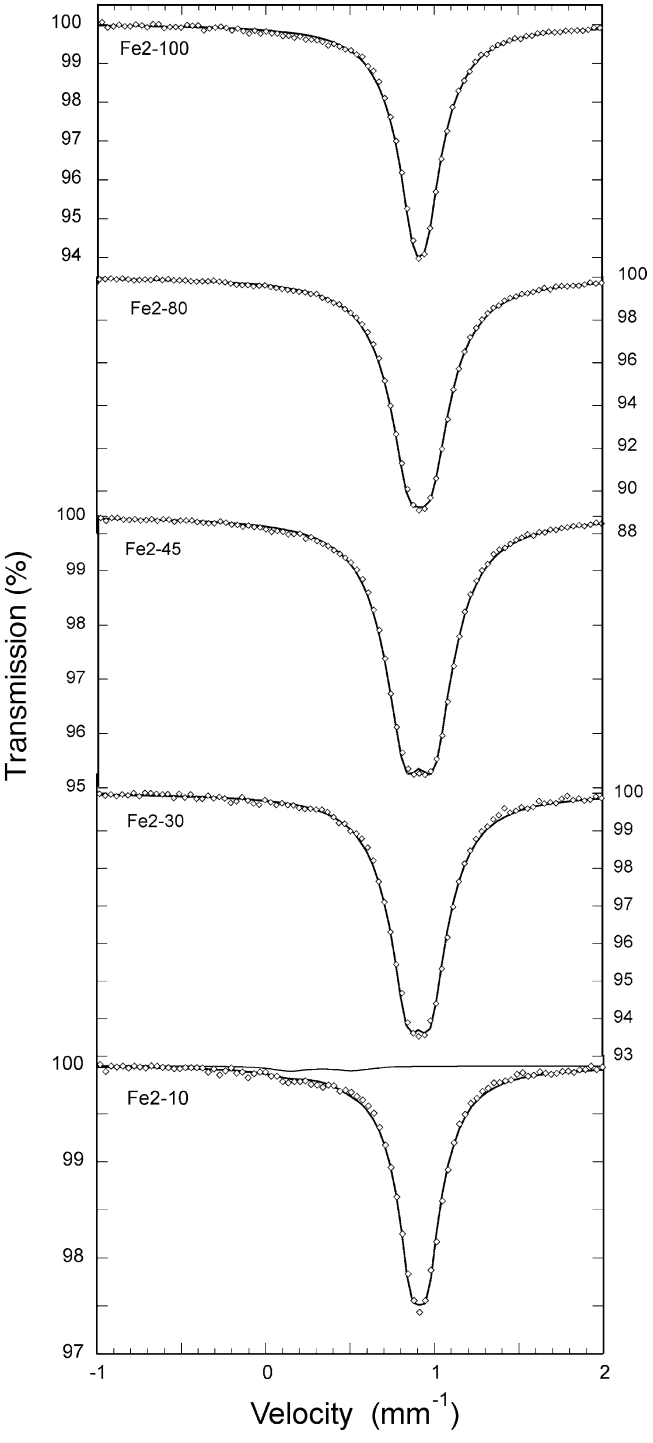

Fig. 5 Mössbauer spectra of spinel samples along the $Fe_xMg_{1-x}Cr_2O_4$ ($0.06 < x < 1.00$) solid-solution series obtained at room temperature. Note weak doublet due to Fe^{3+} in the low-Fe sample (*bottom*)

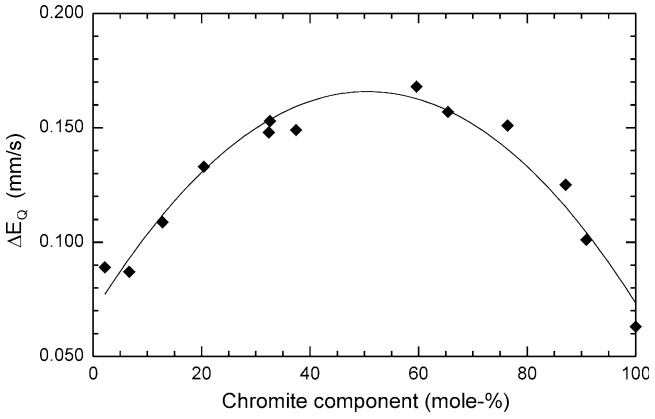

Fig. 6 Observed variation in quadrupole splitting with composition along the $MgCr_2O_4$–$FeCr_2O_4$ series

(Fig. 4), which is tentatively attributed to a spin-allowed *d–d* transition in Cr^{3+} at tetrahedral sites. In contrast to this, spectra of an additional $MgCr_2O_4$ end-member sample (MgCr9), which was synthesized under MgO-oversaturated conditions, do not show these low-energy features (Fig 4).

All Mössbauer spectra are dominated by an absorption line centred at 0.92 mm s^{-1} assigned to Fe^{2+} in the tetrahedral position, in agreement with previous work (e.g. Robbins et al. 1971; Osborne et al. 1983). For compositions close to the Mg-chromite end member, this line is narrow, but towards intermediate compositions the line broadens progressively, and then becomes narrow again towards the chromite end member (Fig. 5). The peak was fitted as a doublet with a small quadrupole splitting which varied continuously over the solid-solution series (Fig. 6). This fitting model is different from that of Osborne et al. (1983), who used a singlet to fit spectra of samples with Mg- and Zn-substituted Cr spinels. Attempts to fit the absorption line in our spectra with a singlet with varying width were less successful, especially for the intermediate composition for which the tip of the absorption lines has a pronounced "flatness", e.g. sample Fe2-45 (Fig. 5). In spectra of the samples with the lowest chromite contents (2 and 6 mol % $FeCr_2O_4$), a weak doublet assigned to Fe^{3+} was also observed (Fig. 5). Due to the low intensity of this doublet, the width, centroid shift and quadrupole splitting were during the fitting procedure constrained to values obtained from samples along the magnesiochromite–magnesioferrite join (Lenaz et al. in preparation). Obtained Mössbauer parameters are listed in Table 3. The Mössbauer data show that iron occurs almost exclusively as $^{IV}Fe^{2+}$ in the present samples. Ferric iron was observed only in samples close to the Mg-chromite end member, and was very minor (< 0.005 apfu). Due to the good counting statistics of the spectra of the more Fe-rich samples, the detection limit of the ferric doublet is judged as low, and the Fe^{3+} concentration can be regarded as being below 0.01 apfu throughout the solid-solution series.

Table 3 Room-temperature Mössbauer parameters for synthetic $(Mg,Fe)Cr_2O_4$ samples. δ Centroid shift (relative α-Fe); ΔE_Q quadrupole splitting; Γ full width at half maximum; A relative area

Sample	Chr comp. (%)	δ (mm^{-1})	ΔE_Q (mm^{-1})	Γ (mm^{-1})	A (%)	Occupancy
Fe2-20	2	0.92	0.09	0.23	81.9	$^{IV}Fe^{2+}$
		0.33	0.37	0.27	18.1	$^{VI}Fe^{3+}$
Fe2-10	7	0.91	0.09	0.23	96.9	$^{IV}Fe^{2+}$
		0.33	0.37	0.27	3.1	$^{VI}Fe^{3+}$
Fe2-10B	13	0.92	0.11	0.25	100	$^{IV}Fe^{2+}$
Fe2-30	20	0.91	0.13	0.26	100	$^{IV}Fe^{2+}$
Fe2-40	33	0.92	0.15	0.26	100	$^{IV}Fe^{2+}$
Fe2-50	32	0.91	0.15	0.28	100	$^{IV}Fe^{2+}$
Fe2-20B	37	0.92	0.15	0.27	100	$^{IV}Fe^{2+}$
Fe2-45	60	0.92	0.17	0.28	100	$^{IV}Fe^{2+}$
Fe2-60	65	0.92	0.16	0.28	100	$^{IV}Fe^{2+}$
Fe2-70	76	0.92	0.15	0.29	100	$^{IV}Fe^{2+}$
Fe2-80	87	0.92	0.13	0.28	100	$^{IV}Fe^{2+}$
Fe2-90	91	0.92	0.10	0.28	100	$^{IV}Fe^{2+}$
Fe2-100	100	0.92	0.06	0.25	100	$^{IV}Fe^{2+}$

Discussion

In the $MgCr_2O_4$–$FeCr_2O_4$ series the observed structural modifications are caused by $Fe^{2+} \rightarrow Mg$ substitution in the T site. The ideal trend between cell parameter and Fe^{2+} content (apfu) is described by the linear relation $a_0 = 8.3325(5) + 0.0442(8)Fe^{2+}$ ($r^2 = 0.99$). The oxygen positional parameter depends on the Fe content according to the linear relation $u = 0.2611(1) + 0.0016(0)Fe^{2+}$ ($r^2 = 0.98$). The linear relation for T–O given by observed values is $T\text{–}O = 1.9645(6) + 0.033(1)Fe^{2+}$ ($r^2 = 0.99$), so that, the calculated Mg tetrahedral bond distance is 1.965(1) Å, while Fe^{2+} tetrahedral bond distance is 1.998(1) Å, which agrees with refined data within the experimental errors.

In spite of significant changes in T–O bond lengths, no influence of tetrahedral cations on M–O distance was detected. However, the changes in T–O bond length, associated with increasing Fe^{2+} content, modify the octahedral unshared edge from 2.952 to 2.969 Å, the octahedral shared edge from 2.683 to 2.662 Å and the O–M–O angle from 84.54° to 83.75°, producing a distortion of the M octahedron.

The small fractions of $^{IV}Cr^{2+}$ observed in optical absorption spectra of some of the Fe-poor samples are too low to be detected by single-crystal diffraction techniques. The increase of the off-diagonal terms in some refinements with intermediate Fe^{2+} compositions may indicate some deviations from the almost isotropic behaviour of the oxygen in stoichiometric spinels. This is probably associated with minute distortions of electric field imposed by the varying occupancy in the nearest tetrahedral sites, as observed also with Mössbauer analyses (ΔE_Q increase).

Optical absorption spectra indicate that chromium is almost exclusively present as a trivalent cation at the

octahedral site. Additional absorption bands attributable to Cr^{2+} and Cr^{3+} at the tetrahedral site are evident in spectra of one of the end-member magnesiochromite samples and solid-solution crystals with the lowest ferrous contents. By taking the recorded absorption coefficient for the spin-allowed band due to $^{IV}Fe^{2+}$ as an approximation for the absorption coefficients for bands due to spin-allowed *d–d* transitions in Cr-cation species at the tetrahedral site, the concentrations of these species (Cr^{2+} and Cr^{3+} at the T site) are calculated to be very low. The highest calculated values are for the end-member magnesiochromite: 0.004 apfu $^{IV}Cr^{2+}$ and 0.014 apfu $^{IV}Cr^{3+}$. From our optical spectra (Figs. 3 and 4), it is evident that the concentration of these Cr species decreases with increasing $^{IV}Fe^{2+}$ content and may be considered negligible in solid-solution crystals with more than 30 mol% chromite component. The occurrence of Cr^{2+} in the tetrahedral site can be regarded as a minor $Cr^{2+}Cr^{3+}{}_2O_4$ component, stabilized by a high activity of chromium during crystal growth. A high activity of chromium can be expected in synthesis experiments with stoichiometric starting compositions, since Cr_2O_3 is less soluble than MgO in the sodium-borate flux.

The optical absorption spectra also indicate, by the absence of the strong and very broad Fe^{2+}–Fe^{3+} intervalence charge transfer bands in the spectral region 9000—14 500 cm^{-1} (Hålenius et al. 2002), that the Fe^{3+} content in the present sample is negligible. This observation confirms the results obtained by Mössbauer spectroscopy.

An observation of spectroscopic interest is the band position of the spin-allowed *d–d* transition in $^{IV}Fe^{2+}$. In spectra of hercynite-spinel solid-solution crystals this feature has a maximum at ~5200 cm^{-1} (Skogby and Hålenius 2003). The observed shift towards lower energies by ca. 500 cm^{-1} (Fig. 7) is consistent with the longer T–O bonds in members of the magnesiochromite-chromite solid solution (1.965–1.996 Å) as compared to the spinel *s.s.*-hercynite solid solution, 1.920–1.968 Å

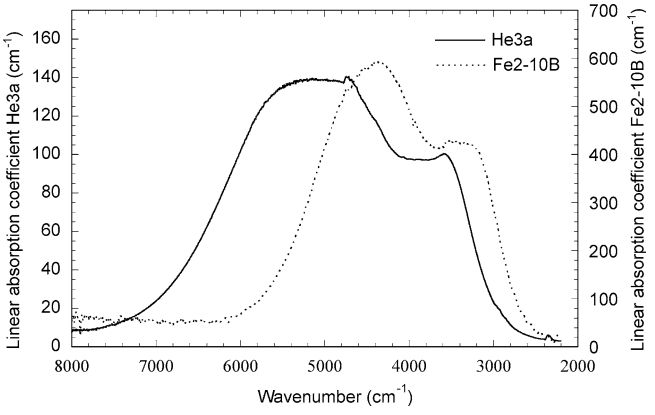

Fig. 7 IR spectra of Fe^{2+}-containing spinel (*He3a* $Fe_{0.11}Mg_{0.89}Al_2O_4$) and magnesiochromite (*Fe2-10b* $Fe_{0.13}Mg_{0.87}Cr_2O_4$). Note difference in band position and absorption

(Andreozzi and Lucchesi 2003). In the crystal-field approximation these bond length differences are predicted to result in a band energy decrease by ca. 9%, which in this case corresponds to ca. 500 cm^{-1}. An additional difference in character of this absorption band between the two solid-solution series is the higher absorption coefficient (ca. 2.5 times) recorded in the present spectra. This demonstrates that next-nearest neighbours may strongly influence the transition moment of spin-allowed electronic *d–d* transitions. The physical causes for the intensification of the $^{IV}Fe^{2+}$ band when substituting Al^{3+} by Cr^{3+} at the neighbouring octahedral sites of the spinel structure are, however, not obvious and need further investigation.

The pronounced increase in ΔE_Q observed for the $^{IV}Fe^{2+}$ quadrupole doublet in Mössbauer spectra of intermediate compositions in the $MgCr_2O_4$–$FeCr_2O_4$ series (Fig. 6) may be related to short range order (SRO) effects. In the spinel structure each T site is surrounded by 12 M sites (second coordination sphere at ca. 3.43 Å) and four neighbouring T sites (fourth coordination sphere at ca. 3.58 Å). All faces of a tetrahedron are turned towards a face of one neighbouring tetrahedron and octahedra are not directly interposed between these T neighbours. The screening action of oxygen ligands is in this way at a minimum between T-site cations and variations in T–T repulsion may cause changes in the electric field at T sites in spite of the relatively long T–T distance. The present samples have all M sites fully occupied by Cr^{3+} and consequently asymmetrical electric fields at the T sites cannot be a direct effect of SRO at the M sites. However, SRO associated with tetrahedral configurations produces also asymmetrical electrical fields around T sites. In the present samples five different neighbouring tetrahedral configurations (i.e. MgMgMgMg, MgMgMgFe, MgMgFeFe, MgFeFeFe, FeFeFeFe) are possible around each tetrahedron. In the end members of the $MgCr_2O_4$–$FeCr_2O_4$ solid-solution series, the neighbouring tetrahedra are occupied by the same cation, which should provide for a highly symmetrical electric field environment, and a small ΔE_Q value. However, at the midpoint of the series the highest probability for mixed tetrahedral occupancies is expected if random mixing of Mg and Fe over the tetrahedral sites is assumed. Osborne et al. (1983) observed band broadening in a Mössbauer spectrum of $(Mg_{0.5}Fe_{0.5})Cr_2O_4$, which they explained as "ferrous iron feels some effect of tetrahedral site substitution". They concluded, however, on the basis of data retrieved from their single sample, that it was unlikely that the effect would be large enough to cause iron ground-state splitting.

Concluding remarks

Structural parameters a_0, u, T–O increase with chromite content, while M–O bond distance remains nearly constant with an average value equal to 1.995(1) Å,

corresponding to the octahedral bond distance of Cr according to Shannon (1976), O'Neill and Navrotsky (1983) and Lavina et al. (2002). The ideal trend between cell parameter and Fe^{2+} content (apfu) is described by the linear relation $a_0 = 8.3325(5) + 0.0443(8)Fe^{2+}$. T–O bond length for $MgCr_2O_4$–$FeCr_2O_4$ series is described by the linear equation T–O = 1.9645(6) + 0.033(1)Fe^{2+}. Consequently, Fe^{2+} and Mg tetrahedral bond lengths are equal to 1.998(1) Å, and to 1.965(1) Å, respectively, close to the values reported by O'Neill and Navrotsky (1983) and Lavina et al. (2002).

Optical absorption spectra indicate that chromium almost exclusively is present as a trivalent cation at the octahedral site. Additional absorption bands attributable to very low fractions of Cr^{2+} and Cr^{3+} at the tetrahedral site are evident in spectra of end-member magnesiochromite and solid-solution crystals with very low ferrous contents synthesized under low Mg activity.

The Mössbauer and optical absorption spectroscopy data show that iron occurs almost exclusively as $^{IV}Fe^{2+}$ in the present samples. Very low Fe^{3+} concentrations (< 0.005 apfu) were observed by Mössbauer spectroscopy in samples with small chromite components. Mössbauer spectra also indicate that electric field at the T sites is sensitive to short range order at the tetrahedral sites in spinels.

Acknowledgements D.L. thanks the Swedish Museum of Natural History and the financial support through HIGH LAT resources (project number HPRI-CT-2001.00125) within the European Community—Access to Research Infrastructure Action of the Improving Human Potential Programme. H.S. and U.H. acknowledge support from the Swedish Research Council. F. Bosi and an anonymous reviewer are kindly acknowledged for improving the quality of the manuscript. This work was also supported with MURST and Trieste University grants (F.P.; Cristallochimica e reazioni di scambio cationico in spinelli, olivine e pirosseni; COFIN 2001). The Italian C.N.R. financed the installation and maintenance of the microprobe laboratory at the University of Padova. R. Carampin, L. Tauro and L. Furlan are kindly acknowledged for technical support.

References

Andreozzi GB, Lucchesi S (2002) Intersite distribution of Fe^{2+} and Mg in the spinel (sensu stricto)-hercynite series by single-crystal X-ray diffraction. Am Miner 87: 1113–1120

Barnes SJ (2000) Chromite in komatiites, II. Modification during greenschist to mid-amphibolite facies metamorphism. J Petrol 41: 387–409

Barnes SJ, Roeder PL (2001) The range of spinel compositions in terrestrial mafic and ultramafic rocks. J Petrol 42: 2279–2302

Blessing RH, Coppens P, Becker P (1972) Computer analysis of step-scanned X-ray data. J Appl Crystallogr 7: 488–492

Della Giusta A, Carbonin S, Ottonello G (1996) Temperature-dependent disorder in a natural Mg–Al–Fe^{2+}–Fe^{3+} spinel. Mineral Mag 60: 603–616

Dick HJB, Bullen T (1984) Chromian spinel as a petrogenetic indicator in abyssal and alpine-type peridotites and spatially associated lavas. Contrib Mineral Petrol 86: 54–76

Evans BW, Frost BR (1975) Chrome spinels in progressive metamorphism—a preliminary analysis. Geochim Cosmochim Acta 39: 959–972

Fabries J (1979) Spinel-olivine geothermometry in peridotites from ultramafic complexes. Contrib Mineral Petrol 69: 329–336

Fujii T (1977) Fe–Mg partitioning between olivine and spinel. Carnegie Inst Wash, Year Book 76: 563–569

Gaffney ES (1973) Spectra of tetrahedral Fe^{2+} in $MgAl_2O_4$. Phys Rev B8: 3484–3486

Greskovich C, Stubican VS (1966). Divalent chromium in magnesium-chromium spinels. J Phys Chem Solids 27: 1379–1384

Hålenius U, Skogby H, Andreozzi GB (2002) Influence of cation distribution on the optical absorption spectra of Fe^{3+}-bearing spinel *s.s.*-hercynite crystals: evidence for electron transition in $^{IV}Fe^{2+}$–$^{VI}Fe^{3+}$ clusters. Phys Chem Miner 29: 319–330

Infante C, Fender BEF (1973) Off-center displacements in spinels: a neutron diffraction examination of $MgCr_2O_4$. J Phys C 6: L333–L336

Irvine TN (1965) Chromian spinel as a petrogenetic indicator, part I. Theory. Can J Earth Sci 2: 648–672

Irvine TN (1967) Chromian spinel as a petrogenetic indicator, Part II. Petrological applications. Can J Earth Sci 4: 71–103

Jernberg P, Sundqvist T (1983) A versatile Mössbauer analysis program. Uppsala University, Institute of Physics (UUIP-1090)

Kamenetsky V (1996) Methodology for the study of melt inclusions in Cr-spinel, and implications for parental melts of MORB from FAMOUS area. Earth Planet Sci Lett 142: 479–486

Kamenetsky V, Crawford AJ, Meffre S (2001) Factors controlling chemistry of magmatic spinel: an empirical study of associated olivine, Cr-spinel and melt inclusions from primitive rocks. J Petrol 42: 655–671

Lavina B, Salviulo G, Della Giusta A (2002) Cation distribution and structure modelling of spinel solid solutions. Phys Chem Miner 29: 10–18

Lenaz D, Skogby H (2003) Flux growth of synthetic single crystal spinels in the (Mg, Fe^{2+})(Cr, Fe^{3+})$_2O_4$ system. Per Miner 72: 69–78

O'Neill HStC (1981) The transition between spinel lherzolite and garnet lherzolite, and its use as a geobarometer. Contrib Miner Petrol 77: 185–194

O'Neill HStC, Dollase WA (1994) Crystal structures and cation distributions in simple spinels from powder XRD structural refinements: $MgCr_2O_4$, $ZnCr_2O_4$, Fe_3O_4 and the temperature dependence of the cation distribution in $ZnAl_2O_4$. Phys Chem Miner 20: 541–555

O'Neill HStC, Navrotsky A (1983) Simple spinels: crystallographic parameters, cation radii, lattice energies, and cation distribution. Am Mineral 68: 181–194

O'Neill HStC, Navrotsky A (1984) Cation distributions and thermodynamic properties of binary spinel solid solutions. Am Mineral 69: 733–753

O'Neill HStC, Wall VJ (1987) The olivine-orthopyroxene-spinel oxygen geobarometer, the nickel precipitation curve, and the oxygen fugacity of the Earth's upper mantle. J Petrol 28: 1169–1191

Osborne MD, Fleet ME, Bancroft GM (1983) Mössbauer study of Mg, Zn substituted Cr-spinel. Solid State Comm 48 (8): 663–664.

Peltonen P, (1995) Crystallization and re-equilibration of zoned chromite in ultramafic cumulates, Vammala Ni-belt, southwestern Finland. Can Mineral 33: 521–535

Poole CP (1964) The optical spectra and color of chromium-containing solids. J Phys Chem Solids 25: 1169–1182

Robbins M, Wertheim GK, Sherwood RC, Buchanan DNE (1971) Magnetic properties and the site distributions in the system $FeCr_2O_4$–Fe_3O_4 ($Fe^{2+}Cr_{2-x}Fe_x{}^{3+}O_4$)

Sack RO, Ghiorso MS (1991) Chromian spinels as petrogenetic indicators: thermodynamics and petrological applications. Am Mineral 76: 827–847

Scowen PAH, Roeder PL, Helz RT (1991) Reequilibration of chromite within Kilauea Iki lava lake, Hawaii. Contrib Mineral Petrol 107: 8–20

Shannon RD (1976) Revised effective ionic radii and systematic studies of interatomic distances in halides and chalcogenides. Acta Crystallogr (A) 32: 751–767

Sheldrick GM (1993) SHELX-93. Program for crystal structure refinement. University of Gottingen, Germany

Skogby H, Hålenius U (2003) An FTIR study of tetrahedrally coordinated ferrous iron in the spinel-hercynite solid solution. Am Mineral 88: 489–492

Slack GA, Ham FS, Chrenko RM (1966) Optical absorption spectra of tetrahedral Fe^{2+} ($3d^6$) in cubic ZnS, CdTe and $MgAl_2O_4$. Phys Rev 152:376–402

Taran MN, Langer K, Platonov AN, Indutny VV (1994) Optical absorption investigation of Cr^{3+} ion-bearing minerals in the temperature range 77–797 K. Phys Chem Miner 21: 360–372

Tokonami M (1965) Atomic scattering factor for O^{-2}. Acta Crystallogr 19: 486

Urusov VS (1983) Interaction of cation on octahedral and tetrahedral sites in simple minerals. Phys Chem Miner 9: 1–5